Medical Infrared Imaging of Normal and Dysplastic Elbows in Dogs

Lauren McGowan[1], Catherine A Loughin[1], Dominic J. Marino[1], Scott E. Umbaugh[2], Peng Liu[2], Maryam Amini[2], Patrick Solt[2], Martin L. Lesser[3], and Meredith Akerman[3]

[1]Department of Surgery, Long Island Veterinary Specialists, Plainveiw, New York ,[2]Department of Electrical and Computer Engineering, School of Engineering, Southern Illinois University, Edwardsville, Illinois and [3]Department of Molecular Medicine and Department of Population Health, Biostatistics Unit, The Feinstein Institute for Medical Research, Hofstra North Shore-LIJ School of Medicine, New Hyde Park, New York

Corresponding Author
Dominic J. Marino
Long Island Veterinary Specialists
163 South Service Road
Plainview, NY 11803
dmarino@livs.org

Submitted May 2014
Accepted June 2015

DOI:10.1111/vsu.12372

Objective: To investigate the ability of medical infrared imaging to differentiate between normal canine elbows and those with abnormal elbows (elbow dysplasia).
Study Design: Prospective cohort study.
Animals: Dogs with normal (n = 15) and abnormal (n = 14) elbows.
Methods: Infrared imaging was performed on all dogs and data analyzed via descriptive statistics and image pattern analysis software. Animals with elbow dysplasia had arthroscopic procedures to confirm the presence of elbow disease.
Results: Computer recognition pattern analysis was up to 100% correct in identifying abnormal elbows and normal elbows, with the medial images most consistent. The caudal, lateral, and cranial images correctly identified 83–100% abnormal elbows. The caudal and lateral images correctly identified 83% normal elbows. A significant difference in temperature was found between normal and abnormal elbows for the cranial full region of interest, lateral images, and each quadrant.
Conclusion: Medical infrared imaging was able to correctly identify known abnormal and known normal elbows in dogs.

Canine elbow dysplasia is one of the leading causes of forelimb lameness in the dog. It is a generalized term used to describe several abnormalities that differ in pathophysiology but that all contribute to structural and functional elbow abnormalities. These abnormalities include fragmented coronoid process, osteochondritis dissecans of the distal humerus, ununited anconeal process, and joint incongruity.[1–4] Certain breeds have a genetic predisposition for elbow dysplasia.[1,5]

Making a diagnosis of elbow dysplasia can be challenging and localizing the site of pain to the elbow can be difficult when a dog has subtle lameness or clinical signs. The diagnostic capabilities of radiographs are highly dependent on position,[2,6,7] and radiographs can be described as normal in dogs with elbow disease and lameness.[8] Computed tomography (CT) and arthroscopy are more accurate than radiographs in the diagnosis of elbow dysplasia but can be expensive and require general anesthesia.[6–9] Previous reports have identified CT as the gold standard for evaluation of elbow dysplasia but more recent studies indicate that arthroscopy is more sensitive and specific for diagnosis.[7,8,10,11] Less frequently utilized modalities, such as magnetic resonance imaging (MRI) and nuclear scintigraphy, are useful in detecting elbow dysplasia.[12,13] Both of these modalities require specialized equipment that may not be readily available, require general anesthesia, and are expensive to acquire.

Medical infrared imaging, also known as thermography, is a noninvasive screening tool used in people and animals to detect abnormal physiologic changes associated with disease.[14–19] Medical infrared imaging measures and displays a visual image of infrared radiation emitted by the body surface. Typically, the infrared image is a color map where warmer colors (white, red, orange, and yellow) represent areas of elevated temperature (e.g., those associated with inflammation, increased circulation or metabolic rate), and cooler colors (green, blue, and black) represent areas of decreased tissue temperature or perfusion (e.g., vascular shunt, infarction, or change in autonomic nervous system).[15,19,20] The change in superficial heat is responsible for changes in the color map, not the heat from deeper tissue.[15,17] The superficial heat detected by the infrared camera is related to sympathetic nerve control of skin blood flow (depth ~5 mm) and the increase and decrease of postganglionic pressure that regulates microdermal blood flow. This is linked to the central nervous system and reflects thermatomal changes relating to deeper structures and functions. Thus medical infrared imaging can be used in subjects of all sizes, regardless of body fat percentage.

New infrared imaging systems incorporate focal plane array detectors with high-speed images and spatial resolution. Image recognition software allows objective analysis of thermal patterns.[17] Medical infrared imaging is used in

Veterinary Surgery 44 (2015) 874–882

people for screening orthopedic conditions,[21–28] neurologic injuries,[29–31] neoplasia,[16,32] and vascular disorders.[20,33,34] Medical infrared imaging can detect changes in the thermal pattern before changes are noted on radiographs.[25,35]

Medical infrared imaging has been reported mostly for use in large animals, such as llamas, cattle, and horses, to aid in diagnosis of infectious,[36,37] reproductive,[38,39] orthopedic,[15,40] and neurologic conditions.[39,41,42] Other reports describe normal patterns in healthy dogs,[43] differentiation of cranial cruciate ligament deficient stifles from normal stifles in dogs,[44] and intervertebral disc disease in chondrodystrophic dogs.[45]

Medical infrared imaging is a non-invasive modality and of low cost to the owner. There is no exposure to ionizing radiation and no adverse effects. Thus, infrared imaging offers advantages as a screening tool for detection of disease. The purpose of this prospective study was to establish a thermal pattern for abnormal elbows in dogs with elbow dysplasia, and to compare to the pattern from normal elbows of dogs. This study also assessed the ability of medical infrared imaging with computerized image recognition pattern analysis to correctly identify abnormal elbows. The mean temperature of various regions of interest (ROI) between abnormal and normal elbows was compared for statistical significance.

MATERIALS AND METHODS

Selection of Cases

All adult dogs presenting with forelimb lameness were initially included. Each dog had a physical, orthopedic, and radiographic examination. Dogs with radiographic evidence suggestive of elbow dysplasia were confirmed via arthroscopy and were included in this study. Dogs were excluded if there was evidence of neurologic or concurrent orthopedic disease. Fifteen dogs (6 Labrador retrievers, 6 golden retrievers, and 3 Bernese mountain dogs; 3 spayed female, 9 neutered male, 2 entire male, 1 entire female) with a median body weight of 36 kg (range 28–48), and a median age of 24 months (range 6–122) were selected for the study. All dogs had elbow effusion and acute or chronic onset of non-weight bearing to partial-weight bearing lameness. Eight of 15 dogs had forelimb muscle atrophy. Hematologic and serum biochemistry were within reference intervals. Both elbows were imaged in all dogs and all radiographic and arthroscopic findings were documented (Table 1).

Selection of Controls

Fifteen Labrador retrievers (1 entire male, 14 entire females) from a training–breeding program (Guide Dog Foundation for the Blind, Smithtown, NY) were evaluated as for the cases with physical, orthopedic, and radiographic examinations. Computed tomography was performed and used to confirm each elbow as normal. The dogs had a median body weight of

Table 1 Signalment, Radiographic, and Arthroscopic Findings in 14 Dogs with Elbow Disease

Age (months)	Breed	Sex	Radiographic Findings	Arthroscopic Findings
13	Labrador	MN	Bilateral moderate sclerosis, DJD	Bilateral FCP, grade 3 cartilage lesion,[52] elbow inconguity
122	Golden retriever	MN	Bilateral moderate DJD, elbow inconguity	Bilateral grade 4 cartilage lesion, severe synovitis
29	Bernese	MN	Bilateral severe DJD, elbow inconguity	Bilateral grade 4 cartilage lesion, FCPs
6.5	Labrador	FI	Bilateral severe sclerosis, osteophytosis	Bilateral FCP and OCD; L cartilage lesion grade 3; R cartilage lesion grade 2
11	Labrador	MN	L mild sclerosis R moderate sclerosis	Bilateral elbow incongruity, grade 3 cartilage lesion
10	Golden retriever	MN	R mild elbow sclerosis R shoulder OCD	R FCP, mild synovitis, grade 1 cartilage lesion; R shoulder OCD
11	Bernese	FS	Bilateral moderate sclerosis, DJD	Bilateral elbow incongruity, FCP, grade 4 cartilage lesion, moderate synovitis
34	Golden retriever	MN	Bilateral moderate DJD, elbow inconguity	Bilateral FCP, elbow inconguity, OCD, grade 3 cartilage lesion
11	Bernese	FS	L moderate sclerosis and elbow inconguity R angular limb deformity	L elbow incongruity, grade 4 cartilage lesion
14	Labrador	MN	Bilateral moderate DJD	Bilateral FCP; R grade 2 cartilage lesion; L grade 4 cartilage lesion
60	Labrador	FS	Bilateral moderate DJD	Bilateral FCP, grade 3 cartilage lesion
7	Labrador	MI	Bilateral mild sclerosis	Bilateral FCPs elbow incongruity, grade 3 cartilage lesions
32	Golden retriever	MN	Bilateral severe DJD	Bilateral FCP, elbow incongruity, grade 4 cartilage lesion
12	Golden retriever	MN	Bilateral mild sclerosis	Bilateral elbow incongruity, grade 2 cartilage lesion
12	Golden retriever	MN	L severe sclerosis R mild sclerosis	L FCP, elbow inconguity, grade 4 cartilage lesion; R elbow incongruity, grade 2 cartilage lesion

MN, male neutered; MI, male intact; FS, female spayed; FI, female intact; L, left; R, right; DJD, degenerative joint disease; FCP, fragmented coronoid process; OCD, osteochondrosis dessicans.

27 kg (range 23–35) and a median age of 12.5 months (range 9–15).

Imaging Procedure

All dogs had limited exercise, were maintained in temperature-controlled runs, and imaged in a room at the same 70°F (21°C) temperature. A stand mounted infrared camera (Med 2000 IRIS, Meditherm, Inc., Beaufort, NC) with a focal plane array amorphous silicone microbolometer was used for all images. For real-time data analysis, the camera was connected to a laptop computer. To minimize thermal artifacts from manual contact, trained technicians handled the dogs by the tail and head using latex gloves at all times. To minimize background artifact potentially created by temperature differences in exterior walls, the dogs were placed in front of a uniform interior wall in a custom designed infrared imaging suite. The distance from the camera to the dogs was ∼1.5 m. Medical infrared imaging of right lateral elbow, medial right elbow, left lateral elbow, medial left elbow, cranial elbow, and caudal elbow were obtained (Fig 1A–F). All images were taken with the dog in a standing position. The handler held the dog's paw and gently extended the limb until the medial elbow was clearly visible. The region of the elbow was defined as distal one-third of the humerus to proximal one-third of the radius/ulna. All images were obtained with an intact haircoat.

A software program (Meditherm, Inc.) was used to save, analyze, and review the data. The program was preset at 8°C temperature scale with a 16-shade color map converted from black and white. White and red color maps were chosen to represent warmer temperatures and blue and black color maps to represent cooler temperatures. The program calculated the maximum (max), mean (avg), and minimum (min) temperatures of each image. Custom image recognition software (CVIPtools, Computer Vision and Image Processing Laboratory, Department of Electrical and Computer Engineering, School of Engineering, Southern Illinois University, Edwardsville, IL) was used to perform computer recognition pattern analysis and to compare thermal patterns of abnormal to normal elbows.

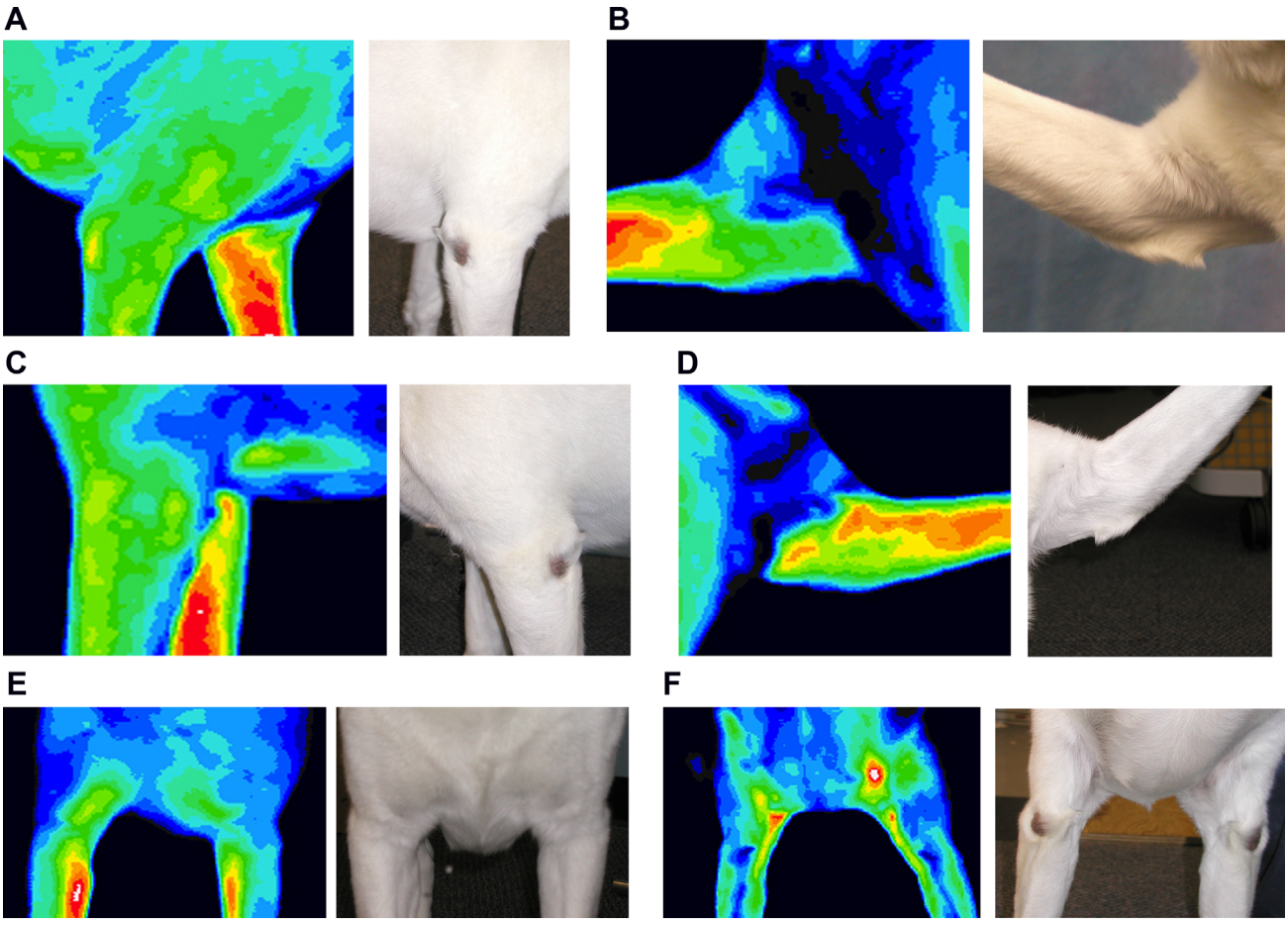

Figure 1 Position of the dog's forelimb (left) with corresponding medical infrared images (right). (A) Right lateral elbow (FRL2). (B) Right medial elbow (MFR2). (C) Left lateral elbow (FLL2). (D) Left medial elbow (MFL2). (E) Left and right cranial elbows (AFLL2, AFLR2). (F) Left and right caudal elbows (PFLL2, PFLR2).

Veterinary Surgery 44 (2015) 874–882

After infrared imaging was complete, all dogs were premedicated with hydromorphone 0.1 mg/kg subcutaneously and atropine 0.4 mg/kg subcutaneously. General anesthesia was induced with telazol 2.2 mg/kg intravenously (IV) and maintained with isoflurane in oxygen via an endotracheal tube. After induction in the controls, CT (Marconi M×8000, Marconi, Medical Systems, Inc., Cleveland, OH) was performed.[46] After induction in the cases, the elbows were prepared for aseptic surgery and elbow arthroscopy was performed with a 2.4-mm, 30° rigid arthroscope (Karl Storz, Tuttlingen, Germany). Thirteen of the 15 cases had bilateral elbow arthroscopy performed without complication. One case had unilateral arthroscopy on a single affected elbow and 1 case had unilateral elbow and shoulder arthroscopy performed on the same limb. All cases were discharged 2 days later and returned for a physical examination at 2 and 8 weeks.

Imaging Pattern Analysis

The CVIPtools software was used to evaluate and analyze the images. Two different experiments were performed to determine which would provide better results. Set I experiments used the standard method for pattern classification and Set II experiments used the standard method and the multilayer perceptron/neural network method. With Set I, different trials were performed, varying the features and the texture distance. The primary differences between the trials were the texture distance and the number of sectors and rings used with the spectral features. With Set II, different pattern classification techniques with all possible combinations of the data normalization and distance metrics were applied on the different views in the image set. Histogram, texture, and spectral features were extracted to training and test sets in different combinations and with texture distance 2 and 6.

An additional analysis of the images was performed. Cross-validation experiments were performed using the "leave-one-out" testing method. Seven sets of experiments were performed with the CVIP-FEPC (CVIP feature extractions and pattern classification tools), with each set having 2,046 permutations, and using K-nearest neighbor as the classification method. The 3 views with the best results from these experiments were then analyzed using the Partek Discovery Suite and linear discriminant analysis.

Experiments were run to classify each segment as a normal elbow or an abnormal elbow. Images from known abnormal elbows and images from known normal elbows were reviewed. The enhanced mask creation software was used for this project. This enhanced software facilitates the creation of a large number of masks. Additionally, algorithms were developed with the CVIP-ATAT (algorithm test and analysis tools) for automatic mask creation. Both the CVIP-ATAT and CVIP-FEPC were performed as previously described.[45] The percentage of abnormal elbows that were correctly identified as abnormal by thermography, and the percentage of normal elbows correctly identified as normal by thermography are reported. Multiple views of thermography were examined and reported. Regions examined: AFLL is the left cranial elbow, AFLR is the right cranial elbow, FLL2 is the left lateral elbow,

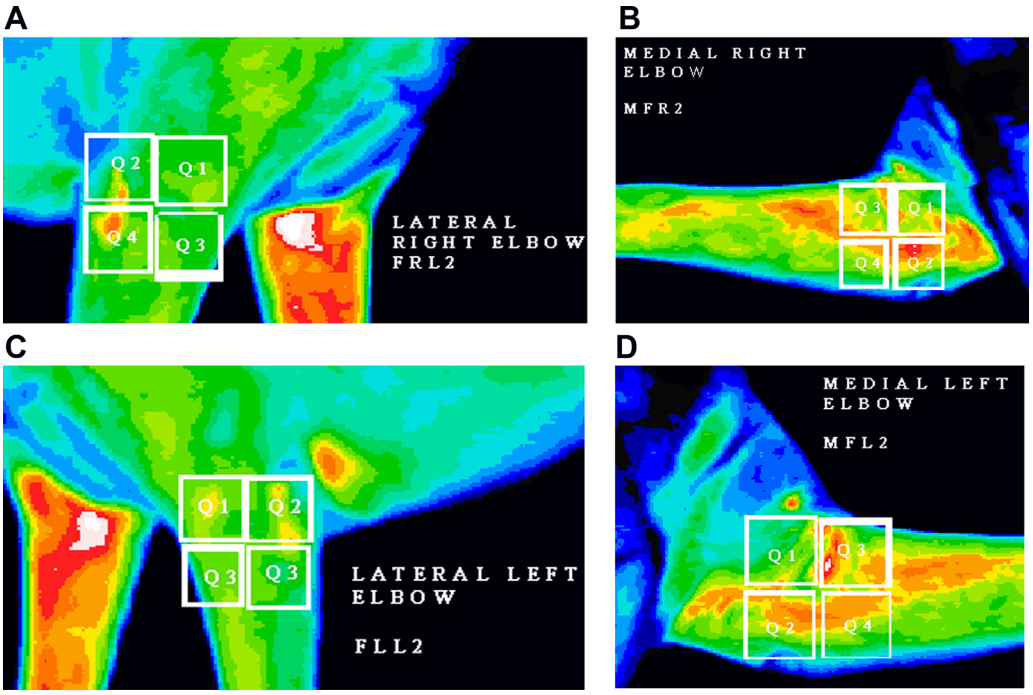

Figure 2 Medical infrared images of the regions of interest. (A) Right lateral elbow (FRL2). (B) Right medial elbow (MFR2). (C) Left lateral elbow (FLL2). (D) Left medial elbow (MFL2). Q, quadrant examined.

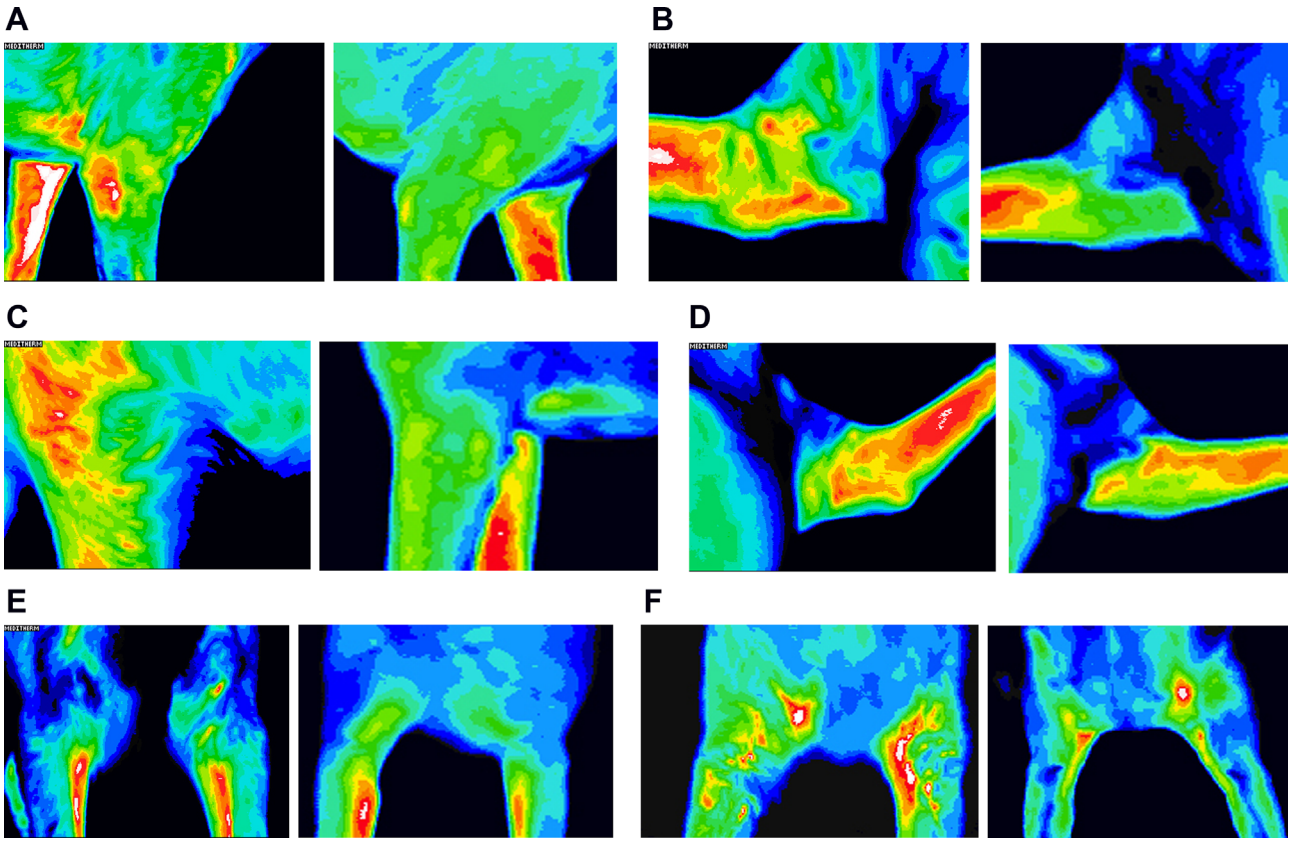

Figure 3 Medical infrared images of abnormal elbows with elbow dysplasia (left) compared to normal elbows (right). (A) Right lateral elbow (FRL2). (B) Right medial elbow (MFR2). (C). Left lateral elbow (FLL2). (D) Left medial elbow (MFL2). (E) Left and right cranial elbows (AFLL2, AFLR2). (F) Left and right caudal elbows (PFL2, PFR2).

FRL2 is the right lateral elbow, MFL2 is the left medial elbow, MFR2 is the right medial elbow, PFL2 is the left caudal elbow, and PFR2 is the right caudal elbow.

Statistical Analysis

The mean and standard deviation (SD) of the temperature identified at each anatomic section was reported for abnormal and normal elbows. The mean of the minimum, maximum, and average temperatures for each region are reported, including AFLLmin, AFLLmax, AFLLavg, AFLRmin, AFLRmax, AFLRavg, FLL2min, FLL2max, FLL2avg, FRL2min, FRL2max, FRL2avg, MFL2min, MFL2max, MFL2avg, MFR2min, MFR2max, and MFR2avg. Temperatures from the caudal regions were not examined. These measurements were nested within dogs. The temperature for regions was compared between abnormal and normal using Student's *t*-test with comparisons made for the full ROI and then per quadrant 1, 2, 3, or 4 (Fig 2). Significance was determined at $P < .05$ for any comparison with no adjustments for multiple testing.

RESULTS

Computer recognition pattern analysis demonstrated a different pattern for abnormal elbows compared to normal elbows.

Table 2 Percentage Correctly Identified Elbows by Standard and Multi-Layer Perceptron Classification Methods

Standard			Multi-Layer Perceptron		
Images	Abnormal Elbow (%)	Normal Elbow (%)	Images	Abnormal Elbow (%)	Normal Elbow (%)
MFR	100	100	MFR	92	92
PFL	100	83	PFL	70	63
FRL	92	83	FRL	91	78

MFR, medial elbow; PFL, caudal elbow; FRL, cranial elbow.

Table 3 Mean (Standard Deviation) Temperature (°C) for the Full Region of Interest (ROI)

FULL ROI			
Region	Normal Elbow	Abnormal Elbow	*P*-Value *t*-test
AFLLmin	24.7 (1.7)	23.3 (1.7)	.029
AFLLmax	30.9 (2.0)	28.6 (1.7)	.002
AFLLavg	27.5 (1.8)	25.6 (1.8)	.005
AFLRmin	24.6 (1.4)	23.4 (1.9)	.056
AFLRmax	30.8 (2.0)	28.5 (2.0)	.003
AFLRavg	27.5 (1.6)	25.9 (1.8)	.016
FLL2min	25.5 (2.0)	23.9 (1.9)	.018
FLL2max	30.0 (1.6)	29.0 (1.9)	.147
FLL2avg	28.1 (1.5)	26.5 (2.0)	.018
FRL2min	25.2 (1.8)	23.8 (2.2)	.055
FRL2max	30.3 (2.4)	28.9 (2.2)	.102
FRL2avg	28.2 (1.6)	26.6 (2.4)	.036
MFL2min	25.9 (1.9)	24.4 (2.3)	.060
MFL2max	31.9 (2.1)	31.2 (2.3)	.369
MFL2avg	29.8 (1.7)	28.2 (2.9)	.076
MFR2min	25.8 (2.0)	24.8 (2.3)	.236
MFR2max	31.9 (1.5)	31.4 (2.3)	.440
MFR2avg	29.7 (1.4)	28.4 (2.6)	.105

AFLL, left cranial elbow; AFLR, right cranial elbow; FLL2, left lateral elbow; FRL2, right lateral elbow; MFL2, left medial elbow; MFR2, right medial elbow; min, minimum temperature; avg, average temperature; max, maximum temperature.

In the lateral images of normal elbows, there was subjectively a more uniform and cooler pattern, mostly shades of green over the epicondyles. The medial image was similar to the lateral image but the patterns were slightly warmer (green to orange). The cranial and caudal images were similar with green to blue patterns along the lateral surfaces and yellow to orange along the medial surfaces. Abnormal elbows had similar but warmer patterns than the normal elbows. The lateral images had an orange to white pattern just caudal to the epicondyles, whereas the epicondyles are green. The medial images also revealed an overall warmer pattern (orange to red) with a small area of green over the epicondyle. The cranial and caudal images were similar to the normal elbows in pattern with warmer color distribution medially (Fig 3A–F).

In Set I, abnormal elbows were correctly identified from thermographic images 100% on the medial images, 83% on the cranial images, and 86% on the lateral images. In Set II, standard results and multi-layer perceptron were compared (Table 2). Identification of abnormal and normal was highest on the medial images and best results were determined using the standard method. With the medial images, abnormal elbows were correctly identified 100% with the standard method and 92% with the multi-layer perceptron technique. With the caudal images, abnormal elbows were correctly identified 100% with the standard method and 83% with the multi-layer perceptron technique. With the lateral images, abnormal elbows were correctly identified 92% with the standard method and 83% with the multi-layer perceptron. Results for normal elbows were best using the standard technique and the multi-layer perceptron technique using the medial images and poorest on the caudal images (Table 2).

Table 4 Mean (Standard Deviation) Temperature (°C) for Each Quadrant

	Quadrant 1			Quadrant 2			Quadrant 3			Quadrant 4		
Region*	Normal	Abnormal	*P*-Value *t*-test	Normal	Abnormal	*P*-Value *t*-test	Normal	Abnormal	*P*-Value *t*-test	Normal	Abnormal	*P*-Value *t*-test
AFLLmin_	25.3 (1.7)	23.7 (1.9)	.019	25.9 (2.1)	25.9 (2.1)	1.000	25.6 (1.5)	23.9 (1.8)	.013	25.8 (2.2)	24.5 (2.3)	.111
AFLLmax_	28.6 (2.1)	26.2 (2.3)	.007	29.3 (2.7)	29.3 (2.7)	1.000	28.6 (2.0)	27.3 (2.0)	.075	29.4 (2.2)	28.2 (1.9)	.140
AFLLavg_	26.9 (2.6)	25.1 (2.1)	.014	27.4 (2.2)	27.4 (2.2)	1.000	27.2 (1.8)	25.7 (1.9)	.042	27.6 (2.0)	26.3 (1.8)	.067
AFLRmin_	25.7 (1.6)	23.3 (1.8)	.001	25.9 (1.6)	24.0 (1.8)	.006	25.4 (1.6)	23.8 (2.1)	.026	25.7 (1.8)	24.2 (1.8)	.033
AFLRmax_	28.4 (1.9)	26.4 (1.9)	.010	29.3 (2.5)	26.8 (2.6)	.011	29.4 (2.5)	27.0 (2.0)	.005	30.0 (2.2)	28.3 (2.3)	.054
AFLRavg_	26.9 (1.8)	25.0 (1.7)	.006	27.5 (2.0)	25.3 (2.0)	.005	27.3 (1.9)	25.6 (1.8)	.018	27.9 (1.9)	26.2 (2.1)	.029
FLL2min	27.2 (1.4)	23.7 (1.9)	.000	26.2 (1.5)	29.2 (1.7)	.000	26.6 (1.5)	24.0 (2.0)	.000	26.2 (1.5)	26.7 (2.1)	.475
FLL2max	29.3 (1.7)	26.2 (2.3)	.000	29.2 (1.7)	27.6 (1.5)	.008	29.4 (1.6)	27.8 (2.1)	.029	29.9 (1.9)	24.1 (2.0)	.000
FLL2avg	28.3 (1.5)	25.1 (2.1)	.000	27.6 (1.5)	26.6 (1.5)	.114	28.5 (1.5)	26.7 (2.1)	.009	28.2 (1.6)	28.2 (2.1)	.953
FRL2min	27.3 (1.4)	25.1 (2.6)	.008	26.3 (1.4)	26.3 (1.4)	1.000	27.2 (1.6)	24.5 (2.8)	.003	25.7 (1.8)	23.9 (2.4)	.024
FRL2max	29.2 (1.7)	27.8 (2.3)	.083	28.9 (1.9)	28.9 (1.9)	1.000	29.4 (1.7)	28.5 (2.0)	.198	30.2 (2.4)	28.4 (2.4)	.041
FRL2avg	28.2 (1.6)	26.6 (2.5)	.042	27.6 (1.5)	27.6 (1.5)	1.000	28.5 (1.6)	26.8 (2.4)	.033	28.2 (1.8)	26.2 (2.6)	.021
MFL2min	26.0 (2.0)	24.4(2.5)	.051	27.2 (1.7)	27.2 (1.7)	1.000	26.2 (1.9)	24.4 (3.0)	.059	27.2 (2.0)	25.4 (2.0)	.017
MFL2max	31.0 (2.2)	30.4 (3.0)	.577	30.9 (2.2)	30.9 (2.2)	1.000	31.4 (2.2)	31.1 (2.5)	.755	30.8 (2.1)	30.6 (2.4)	.819
MFL2avg	28.6 (1.9)	27.2 (3.0)	.142	29.7 (2.1)	29.7 (2.1)	1.000	29.7 (1.8)	28.8 (2.7)	.292	29.6 (1.9)	28.6 (2.6)	.245
MFR2min	25.9 (1.6)	24.4 (2.3)	.052	27.2 (2.2)	27.2 (2.2)	1.000	25.7 (2.0)	24.7 (2.6)	.274	27.5 (1.9)	25.5 (2.2)	.013
MFR2max	30.7 (2.1)	30.2 (2.7)	.591	31.0 (2.0)	31.0 (2.0)	1.000	31.4 (1.7)	31.0 (2.2)	.558	31.0 (1.7)	30.5 (2.4)	.505
MFR2avg	28.4 (1.8)	27.3 (3.0)	.264	29.6 (1.9	29.6 (1.9)	1.000	29.5 (1.7)	28.8 (2.5)	.391	29.7 (1.7)	28.5 (2.6)	.140

*See Table 3 for legend.

Experiments performed with CVIP-FEPC showed correct identification of abnormal elbows on the medial image for 90%, the cranial image for 85%, and the lateral image for 80%. The linear discriminant revealed a correct identification rate of 95% for the medial image.

There was a statistically significant difference in the temperature between normal and abnormal elbows for multiple ROI and also in the quadrants (Tables 3 and 4).

DISCUSSION

Computer pattern analysis was able to identify abnormal elbows and normal elbows. The medial images provided the best results and consistency for classification of normal versus abnormal elbows in both Set I and Set II studies. In people with lateral epicondylitis or tennis elbow, medical infrared imaging shows a discrete localized area of heat (warmer color pattern) near the lateral epicondyle.[47–49] People exhibit pain and have associated inflammation,[47–49] similar to that in dogs with elbow dysplasia because of synovitis, effusion, and degenerative bone change.[4,6,50,51] The abnormal elbow images in the present study showed similar warmer color patterns and documented temperature increases. Normal infrared images for people show a negative gradient over the epicondyle, which is a colder pattern than the surrounding tissue.[47–49] The thermal pattern images of normal elbows in the present study showed similar cooler patterns and temperatures. In people, medical infrared imaging was able to correctly identify 94–98% of people with lateral epicondylitis.[47,49] The present study showed the standard method of analysis was able to correctly identity 100% of abnormal elbows.

The lateral, cranial, and caudal images were less able than the medial images to allow correct identification of normal and of abnormal. However, the classification of normal, and the classification of abnormal was correct greater than 80% of the time, making these images still useful for assessment, especially if reviewed in conjunction with the medial images. The lesser results with the lateral, cranial, and caudal images may be because of difficulty positioning the dogs to obtain these images. Also, the changes in the thermal pattern in the superficial surfaces on these sides of the limb may have less differentiation. Most of the changes noted with elbow dysplasia are associated with the medial aspect of the elbow. Further studies separating specific diseases associated with dysplasia may reveal different patterns.

Most of the significant differences in regional temperatures between normal and abnormal elbows were noted on the cranial and lateral images. This was true for the full ROI and when the elbow was separated into 4 quadrants. Many other regions were not significantly different and thus temperatures differences between abnormal and normal may be small. We did not separate the abnormal dogs based on specific elbow disease or degree of degeneration. Analysis referent to specific disease or stage of disease may show other results.

Previous studies in people show early stages of joint disease with inflammation have changes on medical infrared imaging without radiographic changes. As the joint disease progressed and cartilage and bone become degenerative, both medical infrared imaging and radiographs showed abnormalities.[25,35] The present study in dogs shows medical infrared imaging can identify dogs with abnormal elbows that have abnormalities on arthroscopy and radiographs. Further studies are needed to determine whether there are specific thermal patterns for specific elbow changes and whether medical infrared imaging can identify changes in dogs that do not yet have changes on radiographs.

A limitation of this study was the fact that we did not control for a specific disease associated with elbow dysplasia or other elbow diseases, such as neoplasia or infection. The degree of joint degeneration, degree of lameness, nor length of haircoat was also not controlled. Further studies to evaluate medical infrared imaging for detection of specific elbow disease, determination of degree of joint degeneration, and to clarify whether the length of hair coat affects the pattern are in the planning stages. No dogs were re-imaged at follow-up examination.

This study shows medical infrared imaging reveals an abnormal thermal pattern in dogs with elbow disease. Computer pattern analysis can classify known abnormal joints correctly up to 100% of the time. Although there are significant temperature differences in some regions between normal and abnormal elbows, temperature differences appear small. Medical infrared imaging is non-invasive and may have a role combined with physical examination to screen dogs for elbow disease.

DISCLOSURE

The authors declare no conflicts of interest related to this report.

REFERENCES

1. Griffon D: Surgical diseases of the elbow, in Tobias KM, Johnston SA (eds): *Veterinary surgery: small animal*. St. Louis, MO, Elsevier Saunders, 2012, pp 724–751
2. Mason DR, Schulz KS, Samii VF, et al: Sensitivity of radiographic evaluation of radio-ulnar incongruence in the dog in vitro. *Vet Surg* 2002;31:125–132
3. Samoy Y, Van Ryssen B, Gielen I, et al: Review of the literature: elbow incongruity in the dog. *Vet Comp Orthop Traumatol* 2006;19:1–8
4. Wind A: Elbow incongruity and developmental elbow diseases in the dog: part I. *J Am Anim Hosp Assoc* 1986;22:711–724
5. Bellumori TP, Famula TR, Bannasch DL, et al: Prevalence of inherited disorders among mixed-breed and purebred dogs: 27,254 cases (1995-2010). *J Am Vet Med Assoc* 2013;242:1549–1555
6. Trostel C, McLaughlin R, Pool R: Canine elbow dysplasia: incidence, diagnosis, treatment, and prognosis. *Compend Contin Educ Pract Vet* 2003;25:763–773

7. Wagner K, Griffon DJ, Thomas MW, et al: Radiographic, computed tomographic, and arthroscopic evaluation of experimental radio-ulnar incongruence in the dog. *Vet Surg* 2007;36:691–698
8. Punke JP, Hulse DA, Kerwin SC, et al: Arthroscopic documentation of elbow cartilage pathology in dogs with clinical lameness without changes on standard radiographic projections. *Vet Surg* 2009;38:209–212
9. Holsworth IG, Wisner ER, Scherrer WE, et al: Accuracy of computerized tomographic evaluation of canine radio-ulnar incongruence in vitro. *Vet Surg* 2005;34:108–113
10. Moores AP, Benigni L, Lamb CR: Computed tomography versus arthroscopy for detection of canine elbow dysplasia lesions. *Vet Surg* 2008;37:390–398
11. Werner H, Winkels P, Grevel V, et al: Sensitivity and specificity of arthroscopic estimation of positive and negative radio-ulnar incongruence in dogs. An in vitro study. *Vet Comp Orthop Traumatol* 2009;22:437–441
12. Baeumlin Y, De Rycke L, Van Caelenberg A, et al: Magnetic resonance imaging of the canine elbow: an anatomic study. *Vet Surg* 2010;39:566–573
13. Cook CR, Cook JL: Diagnostic imaging of canine elbow dysplasia: a review. *Vet Surg* 2009;38:144–153
14. Clark JA, Cena K: The potential of infra-red thermography in veterinary diagnosis. *Vet Rec* 1977;100:402–404
15. Eddy AL, Van Hoogmoed LM, Snyder JR: The role of thermography in the management of equine lameness. *Vet J* 2001;162:172–181
16. Head JF, Elliott RL: Infrared imaging: making progress in fulfilling its medical promise. *IEEE Eng Med Biol Mag* 2002;21:80–85
17. Leandro P: *Meditherm manual of clinical thermology*. Cheyenne, WY, Meditherm, Inc., 2006
18. Purohit R: Use of thermography in veterinary medicine, in Lee MHM, Cohen JM (eds): *Rehabilitation medicine and thermography*. Wilsonville, OR, Impress Publications, 2008, pp 129–141
19. Turner TA: Thermography as an aid to the clinical lameness evaluation. *Vet Clin North Am Equine Pract* 1991;7:311–338
20. Love TJ: Thermography as an indicator of blood perfusion. *Ann N Y Acad Sci* 1980;335:429–437
21. Devereaux MD, Parr GR, Lachmann SM, et al: Thermographic diagnosis in athletes with patellofemoral arthralgia. *J Bone Joint Surg Br* 1986;68:42–44
22. Mangine RE, Siqueland KA, Noyes FR: The use of thermography for the diagnosis and management of patellar tendinitis. *J Orthop Sports Phys Ther* 1987;9:132–140
23. Reilly PA, Clarke AK, Ring EF: Thermography in carpal tunnel syndrome (CTS). *Br J Rheumatol* 1989;28:553–554
24. Will RK, Ring EF, Clarke AK, et al: Infrared thermography: what is its place in rheumatology in the 1990s? *Br J Rheumatol* 1992;31:337–344
25. Collins AJ, Ring F, Bacon PA, et al: Thermography and radiology complimentary methods for the study of inflammatory diseases. *Clin Radiol* 1976;27:237–243
26. de Silva M, Kyle V, Hazleman B, et al: Assessment of inflammation in the rheumatoid knee joint: correlation between clinical, radioisotopic, and thermographic methods. *Ann Rheum Dis* 1986;45:277–280
27. Ring EF: Thermographic and scintigraphic examination of the early phase of inflammatory disease. *Scand J Rheumatol Suppl* 1987;65:77–80
28. Salisbury RS, Parr G, De Silva M, et al: Heat distribution over normal and abnormal joints: thermal pattern and quantification. *Ann Rheum Dis* 1983;42:494–499
29. Doman I, Illes T: Thermal analysis of the human intervertebral disc. *J Biochem Biophys Methods* 2004;61:207–214
30. Fujimoto A, Matsumura A, Nakamura K, et al: Chiari malformation type I associated with familial spastic paraplegia: report of a surgically treated case. *Childs Nerv Syst* 2005;21:336–338
31. Pochaczevsky R: The value of liquid crystal thermography in the diagnosis of spinal root compression syndromes. *Orthop Clin North Am* 1983;14:271–288
32. Gautherie M, Haehnel P, Walter JP, et al: Thermovascular changes associated with in situ and minimal breast cancers. Results of an ongoing prospective study after four years. *J Reprod Med* 1987;32:833–842
33. Pochaczevsky R, Pillari G, Feldman F: Liquid crystal contact thermography of deep venous thrombosis. *Am J Roentgenol* 1982;138:717–723
34. Verheye S, De Meyer GR, Krams R, et al: Intravascular thermography: immediate functional and morphological vascular findings. *Eur Heart J* 2004;25:158–165
35. Varju G, Pieper CF, Renner JB, et al: Assessment of hand osteoarthritis: correlation between thermographic and radiographic methods. *Rheumatology (Oxford)* 2004;43:915–919
36. Colak A, Polat B, Okumus Z, et al: Short communication: early detection of mastitis using infrared thermography in dairy cows. *J Dairy Sci* 2008;91:4244–4248
37. Rainwater-Lovett K, Pacheco JM, Packer C, et al: Detection of foot-and-mouth disease virus infected cattle using infrared thermography. *Vet J* 2009;180:317–324
38. Purohit RC, Hudson RS, Riddell MG, et al: Thermography of the bovine scrotum. *Am J Vet Res* 1985;46:2388–2392
39. Purohit RCCR, Riddell MG, et al: Peripheral neurogenic thermogenic thermoregulation of the bovine scrotum. *Thermol Int* 2007;17:138–142
40. Purohit RC, McCoy MD: Thermography in the diagnosis of inflammatory processes in the horse. *Am J Vet Res* 1980;41:1167–1174
41. Graf von Schweinitz D: Thermographic diagnostics in equine back pain. *Vet Clin North Am Equine Pract* 1999;15:161–177
42. Purohit RC, McCoy MD, Bergfeld WA: Thermographic diagnosis of Horner's syndrome in the horse. *Am J Vet Res* 1980;41:1180–1182
43. Loughin CA, Marino DJ: Evaluation of thermographic imaging of the limbs of healthy dogs. *Am J Vet Res* 2007;68:1064–1069
44. Infernuso T, Loughin CA, Marino DJ, et al: Thermal imaging of normal and cranial cruciate ligament-deficient stifles in dogs. *Vet Surg* 2010;39:410–417
45. Grossbard BP, Loughin CA, Marino DJ, et al: Medical infrared imaging (thermography) of type I thoracolumbar disk disease in chondrodystrophic dogs. *Vet Surg* 2014;43:869–876

46. House MR, Marino DJ, Lesser ML: Effect of limb position on elbow congruity with CT evaluation. *Vet Surg* 2009;38:154–160

47. Binder A, Parr G, Thomas PP, et al: A clinical and thermographic study of lateral epicondylitis. *Br J Rheumatol* 1983;22:77–81

48. Shilo R, Engel J, Farin I, et al: Thermography as a diagnostic aid in tennis elbow. *Handchirurgie* 1976;8:101–103

49. Thomas D, Siahamis G, Marion M, et al: Computerised infrared thermography and isotopic bone scanning in tennis elbow. *Ann Rheum Dis* 1992;51:103–107

50. Trostel C, McLaughlin R, Pool R: Canine elbow dysplasia: anatomy and pathogenesis. *Compend Contin Educ Pract Vet* 2003;25:754–762

51. Wind A, Packard ME: Elbow incongruity and developmental diseases in the dog: part II. *J Am Anim Hosp Assoc* 1986;22:725–730

52. Outerbridge RE: The etiology of chondromalacia patellae. *J Bone Joint Surg Br* 1961;43-B:752–757